Appl Phys B (2011) 103:941–945
DOI 10.1007/s00340-010-4347-5

Applied Physics B
Lasers and Optics

Conversion between anticipating and lag chaos synchronization induced by different bias current levels in mutually delay-coupled semiconductor lasers

J.-T. Shen · C.-R. Fan · J.-G. Wu · G.-Q. Xia · L. Ding · N.-Y. Li · Z.-M. Wu

Received: 14 August 2010 / Revised version: 12 November 2010 / Published online: 18 December 2010

Abstract Based on a mutually delay-coupled semiconductor lasers (SLs) system, through adjusting the bias current of a SL and fixing that of the other one, the conversion between anticipating and lag chaos synchronization of this system has been experimentally observed for the first time. Experimental results show that for two SLs with the similar operation parameters, the SL biased at a relatively higher current level plays a leader role due to its relatively higher output power. Considering that the SL with a higher bias current level will oscillate at a longer wavelength, the SL with a longer wavelength becomes the leader, which provides a synchronization conversion scheme via by purely electronic current drive. Furthermore, the corresponding theoretical analyses have been given, and show that whether the SL with a longer or shorter wavelength becomes the leader mainly depends on the approach of the driving of frequency detuning between the two SLs.

1 Introduction

Chaos and chaos synchronization based on semiconductor lasers (SLs) have attracted considerable attentions due to their attractive applications in high-speed secure communications [1–18], chaotic radar [19], high-speed random bit generation [20, 21] and so on. In 2005, a field experiment on unidirectional optical chaos secure communication has been reported via a metropolitan business area network [1]. Obviously, unidirectional chaos secure communication is not enough. The inevitably developing trend of message transmission should be bidirectional, multidirectional, and even network. Therefore, in recent years, bidirectional optical chaotic secure communication has become a new research focus, and many schemes based on mutually delay-coupled SLs have been proposed [7–14]. For completely symmetrical mutually delay-coupled SLs, the chaos synchronization characteristics behave in an unstable way due to spontaneous symmetry-breaking phenomena [8]. By introducing an additional optical feedback, stable chaos synchronization with zero time delay can be realized [12]. However, the additional optical feedback will make the system more complex. Zhang et al. have proposed an extremely asymmetrically mutually delay-coupled SLs scheme without optical feedback, and the theoretical results showed that the system could realize stable chaos synchronization [13]. However, this extremely asymmetrical mutually delay-coupled SL system requires two SLs with large difference in output power or different optical paths for two different coupled directions.

In this paper, based on a simple mutually delay-coupled scheme constructed by two SLs with similar operation parameters, the stable anticipating or lag chaos synchronization has been firstly experimentally observed under the asymmetrical bias current level of the two similar SLs. The relationship of synchronization state (anticipating and lag synchronization) with the bias level has been investigated. For the two similar SLs used in this experiment, the asymmetrical bias current level will simultaneously result in the fre-

J.-T. Shen · J.-G. Wu · G.-Q. Xia · L. Ding · N.-Y. Li · Z.-M. Wu (✉)
School of Physics, Southwest University, Chongqing 400715, China
e-mail: zmwu@swu.edu.cn

C.-R. Fan
School of Physics, Nankai University, Tianjin 300071, China

G.-Q. Xia
Key Lab of Fiber Sensing and Communications, Ministry of National Education, University of Electronic Science and Technology of China, Chengdu 610054, China

quency detuning and power difference between the two SLs. Experiments show that the SL with a higher bias current, accompanied by a higher power level and a longer oscillation wavelength, will play a leader role. This approach provides an alternative way of synchronization conversion to that in [9] by frequency detuning driven by varying temperature of one of the two SLs. Finally, based on the theoretical model of the mutually delay-coupled SLs, numerically simulated results have been given, which are basically consistent with the experimental results.

2 Experimental setup

Figure 1 shows the schematic of the experimental setup. The output of SL1 (SMSR $>$ 50 dB) passes through the aspheric lens, and then is split into two parts by a beam splitter. One part is injected into SL2 to form the mutually delay-coupled structure after passing through a neutral density filter (NDF) and a beam splitter (BS2), and the other part is sent to the detection system through an optical isolator (OI1) and a fiber coupler (FC1). The output of SL2 experiences a similar process. The flight time τ between the SL1 and SL2 is 3.45 ns. The NDF is used to control coupling strength. The photoelectric detector (PD, New Focus 1544-B, bandwidth 12 GHz) is used to convert the optical signal into an electrical signal. The digital oscilloscope (OSC, Agilent 54855A, bandwidth 6 GHz) is used to record chaotic time series. The optical spectrum analyzer (OSA, Ando AQ6137C) with a wavelength resolution of around 0.01 nm is used to detect optical spectra of the SL. Using the temperature controller (ILX-Lightwave, LDT-5412 with 0.01 K accuracy), the SL1 and SL2 are stabilized at 20.00°C and 20.63°C, respectively. The bias current levels of SLs are driven by an ultra-low-noise and high-accuracy current source (ILX-Lightwave, LDX-3620). During experiments, the current of SL1 (I_1) is fixed at 20.15 mA (approximately 1.81 times threshold current of SL1), and the free running wavelength of the SL1 is $\lambda_1 = 1549.814$ nm. The current of SL2 (I_2) is varied continuously from 18.8 mA to 21.0 mA. For $I_2 = 20.00$ mA (approximately 1.8 times threshold current of SL2), the free running wavelength of the SL2 is the same as that of the SL1 biased at $I_1 = 20.15$ mA.

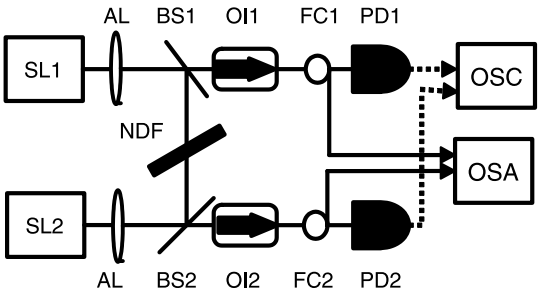

Fig. 1 Experimental setup. SL: semiconductor laser; AL: aspheric lens; BS: beam splitter; OI: optical isolator; NDF: neutral density filter; PD: photo detector; FC: fiber coupler; OSA: optical spectrum analyzer; OSC: digital oscilloscope. The *solid lines* represent optical paths and the *dash lines* represent microwave circuits

3 Experiment results and discussion

Firstly, the coupling optical path is blocked, the free running optical spectra of SL1 can be observed as shown in Fig. 2(a). Next, after connecting the coupling optical path and adjusting the NDF, the output of SL1 in such a mutually delay-coupled system can behave according to a chaotic state, and the output optical spectra of SL1 is shown in Fig. 2(b). Comparing these two spectra, the optical spectrum in the chaotic state is obviously broadened.

To specifically describe the synchronization quality between the two SLs, the quality of chaos synchronization and its time shift can be quantified by calculating the following shifted correlation coefficient $C(\Delta t)$ [4]:

$$C(\Delta t) = \frac{\langle [P_1(t) - \langle P_1 \rangle][P_2(t + \Delta t) - \langle P_2 \rangle] \rangle}{\{\langle [P_1(t) - \langle P_1 \rangle]^2 \rangle \langle P_2(t) - \langle P_2 \rangle]^2 \rangle\}^{1/2}} \quad (1)$$

where subscripts 1 and 2 characterize SL1 and SL2, respectively, Δt is the time shift between two lasers output, the brackets $\langle\,\rangle$ denote temporal averages, P represents chaotic time series. The larger the C value is, the better the synchronization quality between the two lasers is. For perfect chaos synchronization, C equals to 1.

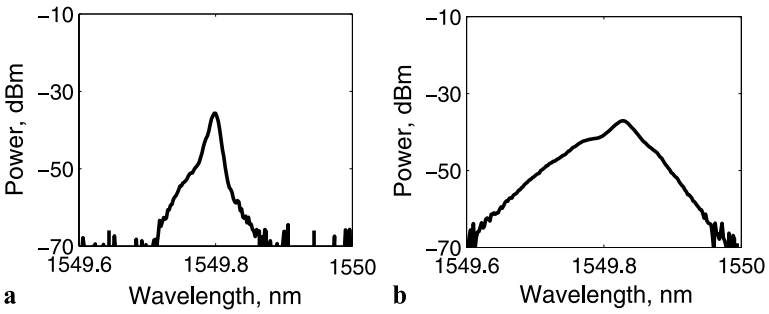

Fig. 2 Output optical spectrum of SL1: (**a**) free running; (**b**) chaotic state

During the experiment, through adjusting I_2 within a small range, the symmetry of the system will be broken down. On the one hand, the variation of I_2 will make the SL2 output power changed, so the relative injected levels will be different between SL1 and SL2. One the other hand, the variation of I_2 will result in frequency detuning between the two SLs, different frequency detuning ($\Delta f = f_1 - f_2$, f_1 and f_2 represent the free running frequencies of SL1 and SL2, respectively) can be obtained through changing I_2. Therefore, after changing I_2, the broken symmetry includes the injection level and frequency match between SL1 and SL2. This is different from the case that the frequency detuning occurred by adjusting the temperature of SL and fixing the current of SL [9], where the output power of the SL does not change obviously with the variation of the temperature of SL. Figure 3 shows the correlation between the frequency detuning Δf of the two SLs and I_2. From this diagram, one can observe that with the increase of I_2, the frequency detuning is varied slowly and linearly.

Figure 4 depicts the chaotic time series and the cross-correlation coefficient for different I_2. From Figs. 4(a3) and 4(b3), there appear two main peaks, respectively, corresponding to the cross-correlation values shifted by the one-way coupling delay of $\Delta t = +\tau$ (called $C(+\tau)$) and $\Delta t = -\tau$ (called $C(-\tau)$). For the case of $I_2 = 19.61$ mA (corresponding frequency detuning is -364 MHz), $C(-\tau)$ is smaller than $C(+\tau)$, so the chaotic time series of SL1 anticipate that of SL2 by τ. However, for the case of $I_2 = 20.41$ mA (the corresponding frequency detuning is 338 MHz), $C(-\tau)$ is larger than $C(+\tau)$, so the chaotic time series of SL1 lag behind that of SL2 by τ. Therefore, for the case of frequency detuning driven by adjusting the bias current level, the SL with the longer wavelength becomes the leader.

Figure 5 shows the dependence of $C(+\tau)$ and $C(-\tau)$ on the I_2 (see Fig. 5(a)) and Δf (see Fig. 5(b)). The solid line represents the fitted curve for $C(+\tau)$ and the dash line represents the fitted curve for $C(-\tau)$. When I_2 is changed from 18.8 mA to 19.86 mA (accordingly, Δf varies from -1.29 GHz to -156 MHz, i.e. $I_2 < I_1$ and $\lambda_1 > \lambda_2$), SL1 anticipates SL2 because of $C(-\tau) < C(+\tau)$. When I_2 is

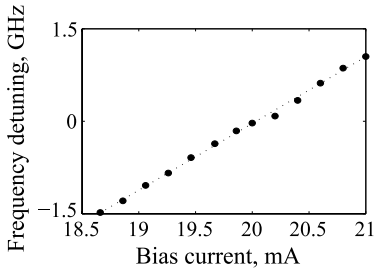

Fig. 3 Correlation between frequency detuning Δf and I_2

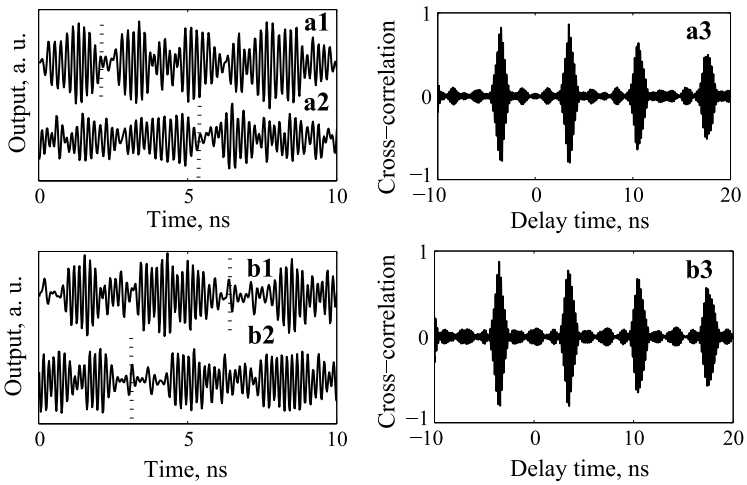

Fig. 4 Chaotic time series and cross-correlation coefficient for $I_2 = 19.61$ mA (**a**) and $I_2 = 20.41$ mA (**b**). (**a1**) and (**b1**) are the chaotic time series of SL1, (**a2**) and (**b2**) is the chaotic time series of SL2, (**a3**) and (**b3**) are the cross-correlation coefficient between the two lasers

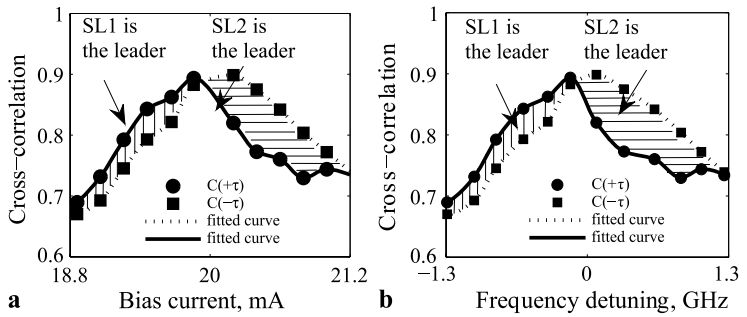

Fig. 5 Dependence of $C(+\tau)$ and $C(-\tau)$ on the I_2 (**a**) and Δf (**b**)

changed from 20.2 mA to 21 mA (accordingly, Δf varies from 836 MHz to 1.05 GHz, i.e. $I_2 > I_1, \lambda_2 > \lambda_1$), SL2 anticipates SL1 because of $C(-\tau) > C(+\tau)$. That is to say, the laser with a larger bias current plays the leader role or the laser with a longer wavelength plays the leader role. By the way, it should be pointed out that the latter conclusion is just drawn for the case that the frequency detuning is driven by varying of the current of SL. If the frequency detuning is driven by varying SL temperature, the SL with a shorter wavelength will become the leader [9].

4 Theoretical simulations and analysis

To confirm our experimental observations, we use a rate equation theoretical model of mutually delay-coupled SLs as follows [8]:

$$\frac{dE_1}{dt} = \frac{1}{2}(1+i\alpha)\left[G_1 - \frac{1}{\tau_p}\right]E_1(t) + \frac{k}{\tau_{\text{in}}}E_2(t-\tau)e^{[-i2\pi(f_2\tau+\Delta f t)]} \quad (2)$$

$$\frac{dE_2}{dt} = \frac{1}{2}(1+i\alpha)\left[G_2 - \frac{1}{\tau_p}\right]E_2(t) + \frac{k}{\tau_{\text{in}}}E_1(t-\tau)e^{[-i2\pi(f_1\tau-\Delta f t)]} \quad (3)$$

$$\frac{dN_{1,2}}{dt} = \frac{I_{1,2}}{q} - \frac{N_{1,2}}{\tau_n} - G_{1,2}|E_{1,2}|^2 \quad (4)$$

where subscripts 1 and 2 represent SL1 and SL2, respectively. E is the slowly varying complex electrical field amplitudes, N is the carrier numbers, α is the line-width enhancement factor, τ_p is the photo lifetime, τ is the delay-coupling time, k is the coupling coefficient, τ_{in} is the round-trip time, f is the frequency, Δf is the frequency detuning, I is the bias current, τ_n is the carrier lifetime, G is optical gain coefficient and can be represented by

$$G_{1,2} = \frac{g_{1,2}(N_{1,2} - N_0)}{1 + \varepsilon|E_{1,2}|^2} \quad (5)$$

where g is differential gain coefficient, N_0 is the transparency carrier number, ε is the gain saturation coefficient.

Equations (2)–(5) can be solved by using the fourth-order Runge–Kutta algorithm. During the simulations, the used data of the parameters are $\alpha = 3$, $\tau_n = 2.25$ ns, $\tau_p = 2$ ps, $\tau_{\text{in}} = 8$ ps, $g = 8.9 \times 10^{-6}$ ns^{-1}, $\varepsilon = 1 \times 10^{-7}$, $\tau = 3.45$ ns, $N_0 = 1 \times 10^8$, $I_1 = 20.15$ mA, Δf is varied with I_2 and the correlation between them has been given in Fig. 3.

Figure 6 depicts the relationship between $C(\tau)$ and $C(-\tau)$ with I_2 (Fig. 6(a)) and Δf (Fig. 6(b)). From Fig. 6(a), it can be seen that $C(+\tau) > C(-\tau)$ for increasing I_2 from 18.8 mA to 20 mA ($\approx I_1$) but $C(+\tau) < C(-\tau)$ for increasing I_2 from 20 mA to 21 mA. Therefore, the SL with a larger bias current level becomes the leader. Based on Fig. 6(b), the SL with a longer wavelength will be the leader. The above simulated results are the same as the experimental results.

In order to determine which laser will play the leader role under different conditions, Fig. 7 gives the dependence of

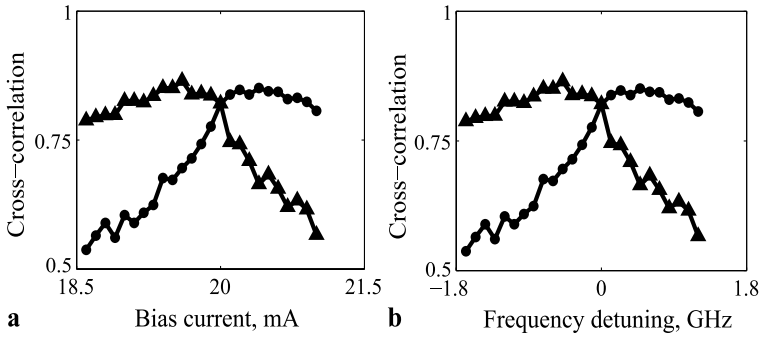

Fig. 6 Dependence of $C(+\tau)$ and $C(-\tau)$ with I_2 (**a**) and Δf (**b**). The *triangle line* represents $C(+\tau)$ and the *dotted line* represents $C(-\tau)$

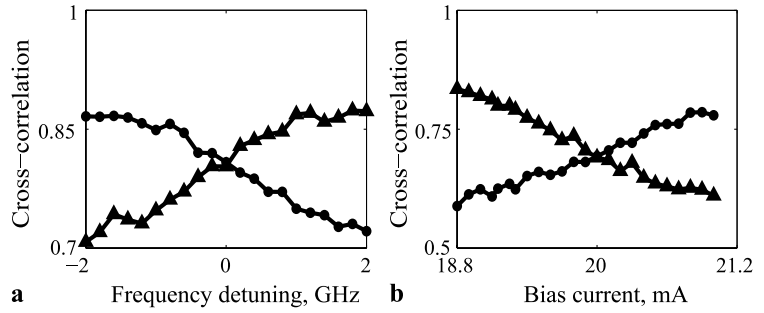

Fig. 7 Dependence of $C(+\tau)$ and $C(-\tau)$ on Δf (**a**) and I_2 (**b**), where (**a**) is for fixing the laser current and changing the laser temperature and (**b**) is for changing the current but without frequency detuning

$C(+\tau)$ and $C(-\tau)$ on I_2 and Δf, where Fig. 7(a) is for fixing the current and changing the temperature of SL2 and Fig. 7(b) is for changing current of SL2 but without frequency detuning. Through adjusting the temperature of SL2 but fixing the current of SLs, a different frequency detuning can also be obtained. The results show that the SL with short wavelength will be the leader, which has been proved experimentally [9]. For the case of changing the current but without frequency detuning (see Fig. 7(b)), the SL with a larger bias current level becomes the leader due to its larger output power. Comparing Fig. 7(b) with Fig. 6(a), it can be deduced that the power asymmetry is the key factor to determine which one is the leader when the system simultaneously exists with asymmetrical power and asymmetrical frequency. Therefore, the SL with a longer wavelength becomes the leader for the currents of two SLs that are asymmetrical and the two SLs temperatures are fixed, but the opposite results will be obtained once the bias current levels of the two SLs are approximately identical but the two SL temperature are asymmetrical.

5 Conclusions

Based on a simple mutually delay-coupled system of SLs, the chaos synchronization states including anticipating and lag synchronization for the two lasers with different bias current levels are experimentally investigated for the first time. The experimental results show that the conversion between anticipating and lag chaos synchronization can be achieved by varying the bias current levels of the two SLs. Furthermore, based on the rate equation theoretical model of such a mutually delay-coupled SLs system, the synchronization characteristics of this system have been simulated. The theoretical results are similar to the experimental results.

Acknowledgements This work was supported by the National Natural Science Foundation of China under Grant Nos. 60978003, 61078003 and 11004161, the National Natural Science Foundation of Chongqing City under Grant No. 2010BB9125, the Fundamental Research Funds for the Central Universities under Grant Nos. XDJK2009B010 and XDJK2010C21, and the Open Fund of the Key Lab of Fiber Sensing and Communications, Ministry of National Education of China.

References

1. A. Argyris, D. Syvridis, L. Larger, V. Annovazzi-Lodi, P. Colet, J. García-Ojalvo, C.R. Mirasso, L. Pesquera, K.A. Shore, Nature **437**, 343 (2005)
2. Y. Liu, H.F. Chen, J.M. Liu, P. Davis, T. Aida, Phys. Rev. Lett. **63**, 031802 (2001)
3. I.V. Koryukin, P. Mandel, Phys. Rev. E **65**, 026201 (2002)
4. J.M. Buldú, J. García-Ojalvo, M.C. Torrent, IEEE J. Quantum Electron. **40**, 640 (2004)
5. G.Q. Xia, Z.M. Wu, J.G. Wu, Opt. Express **13**, 3445 (2005)
6. J.G. Wu, G.Q. Xia, X. Tang, X.D. Lin, T. Deng, L. Fan, Z.M. Wu, Opt. Express **18**, 6661 (2010)
7. T. Deng, G.Q. Xia, L.P. Cao, J.G. Chen, X.D. Lin, Z.M. Wu, Opt. Commun. **282**, 2243 (2009)
8. T. Heil, I. Fischer, W. Elsässer, Phys. Rev. Lett. **86**, 795 (2001)
9. S. Sivaprakasam, P.S. Spencer, P. Rees, K.A. Shore, Opt. Lett. **27**, 1250 (2002)
10. M.C. Chiang, H.F. Chen, J.M. Liu, Opt. Commun. **261**, 86 (2006)
11. N. Gross, W. Kinzel, I. Kanter, M. Rosenbluh, L. Khaykovich, Opt. Commun. **267**, 464 (2006)
12. E. Klein, N. Gross, M. Rosenbluh, W. Kinzel, L. Khaykovich, I. Kanter, Phys. Rev. E **73**, 066214 (2006)
13. W.L. Zhang, W. Pan, B. Luo, X.H. Zou, M.Y. Wang, Z. Zhou, Opt. Lett. **33**, 237 (2008)
14. P. Rees, P.S. Spencer, I. Pierce, S. Sivaprakasam, K.A. Shore, Phys. Rev. E **68**, 033818 (2003)
15. J.G. Wu, G.Q. Xia, Z.M. Wu, Opt. Express **17**, 20124 (2009)
16. L. Larger, P.A. Lacourt, S. Poinsot, V. Udaltsov, Laser Phys. **15**, 1209 (2005)
17. J. Liu, Z.M. Wu, G.Q. Xia, Opt. Express **17**, 12619 (2009)
18. Z.C. Gao, Z.M. Wu, L.P. Cao, G.Q. Xia, Appl. Phys. B **97**, 645 (2009)
19. F.Y. Lin, J.M. Liu, IEEE J. Quantum Electron. **40**, 815 (2004)
20. A. Uchida, K. Amano, M. Inoue, K. Hirano, S. Naito, H. Someya, I. Oowada, T. Kurashige, M. Shiki, S. Yoshimori, K. Yoshimura, P. Davis, Nat. Photon **2**, 728 (2008)
21. I. Kanter, Y. Aviad, I. Reidler, E. Cohen, M. Rosenbluh, Nat. Photon **4**, 58 (2010)